Okiemute Dickson Ofuyekpone[1], Ngozi Grace Emordi[2], Ochuko Goodluck Utu[3], Basil O. Onyekpe[4], Adeolu Adesoji Adediran[5,6]*

[1]Department of Materials and Metallurgical Engineering, Faculty of Engineering, Southern Delta University, Ozoro, NigeriaM [2]Department of Mechatronics Engineering, Faculty of Engineering, University of Delta, Agbor, Nigeria, [3]Department of Welding Engineering Technology, Delta State Polytechnic, Ogwashi-Uku, Nigeria, [4]Department of Materials and Metallurgy, Faculty of Engineering, University of Benin, Benin City, Nigeria, [5]Materials Design and Structural integrity Group, Department of Materials and Metallurgical Engineering, Federal University, Oye-Ekiti, Ekiti State, Nigeria, [6]Department of Mechanical Engineering Science. University of Johannesburg, South Africa

Scientific paper
ISSN 0351-9465, E-ISSN 2466-2585
https://doi.org/10.62638/ZasMat1780

Zastita Materijala 67 ()
(2026)

Corrosion mitigation of alloy 304L in HCl solution using an environmentally compatible and sustainable extract

ABSTRACT

The corrosion inhibition performance of Stylosanthes gracilis (SG) leaf extract on Alloy 304L stainless steel in 1.0 M HCl was investigated using gravimetric, electrochemical, GC–MS, adsorption, and SEM/EDX analyses. Results showed that the extract effectively reduced corrosion through the formation of a protective adsorbed film on the alloy surface. Corrosion rate and current density decreased with increasing extract concentration, while inhibition efficiency and polarization resistance increased significantly, reaching a maximum efficiency of about 94.6% at 1.2 g/L. The corrosion potential shift of 0.069 V indicated mixed-type inhibition behaviour. Adsorption studies revealed spontaneous adsorption following the Langmuir isotherm through combined physisorption–chemisorption mechanisms. Kinetic and residual analyses showed that the second-order model best described the inhibition process, suggesting cooperative adsorption interactions among phytochemical constituents. GC–MS analysis identified oxygen-, sulfur-, nitrogen-, and phosphorus-containing compounds responsible for adsorption and hydrophobic barrier formation. SEM/EDX results confirmed substantial reduction in chloride-induced surface degradation. The study demonstrates the long-term corrosion protection capability and industrial potential of SG extract as a sustainable green inhibitor for stainless steel in acidic environments.

Keywords: *Corrosion inhibition, electrochemical techniques, Alloy 304L, 1.0M HCl, Stylosanthes gracilis extract*

1. INTRODUCTION

Corrosion is an inevitable electrochemical process through which metals and their alloys interact with their surrounding environment, leading them toward a more thermodynamically stable state [1-4]. It has been experimentally proven and established that Iron, carbon, and a few other minuscule chemicals make up steel, and the presence of chemically reactive iron leads to corrosion [5]. The rusting process starts when oxygen and water come into contact with chemically reactive iron.

Despite significant advances in materials engineering, corrosion remains a major challenge in critical industries such as chemical processing, petrochemical operations, fertilizer production, and metallurgy, resulting in substantial economic losses worldwide [1-4].

Austenitic stainless steels are widely employed due to their excellent corrosion resistance, mechanical strength, ease of fabrication, aesthetic appeal, and resistance to product contamination. These attributes make them suitable for applications in industrial plants, marine environments, and architectural structures. Additionally, austenitic stainless steels retain high strength and toughness even at low temperatures. However, while these steels perform well in environments where anodic and cathodic reactions are freely distributed across the surface, they are

Corresponding author: *Okiemute Dickson Ofuyekpone*
E-mail: okedickbest@yahoo.com
Paper received: 09. 02.2026.
Pape corrected: 20.05.2026.
Pape accepted: 11. 06. 2026.

highly susceptible to corrosion in aggressive media such as hydrochloric acid, where localized electrochemical reactions dominate [1-2].

Hydrochloric acid and other mineral acids are extensively used in industrial processes including scale removal, rust cleaning, boiler and heat-exchanger maintenance, and chemical or electrochemical etching [6]. In the oil and gas sector, hydrochloric acid and hydrogen sulfide are commonly generated from the hydrolysis of calcium and magnesium chlorides during crude oil processing and steam stripping. These corrosive species accumulate in the aqueous phase of overhead condensers, where hydrochloric acid is primarily responsible for severe metallic degradation [6-7].

The presence of chloride ions significantly accelerates corrosion by destabilizing the protective passive film on stainless steel surfaces. Chloride ions penetrate and adsorb onto the oxide layer, displacing passivating species and facilitating the migration of ferrous ions from the metal surface. This process ultimately results in film breakdown, localized anodic site formation, and rapid metal dissolution. The corrosion-accelerating role of chloride ions involves multiple mechanisms, including oxide film penetration, complex formation with iron ions, and catalytic bridging effects [6-9].

To mitigate such degradation, corrosion inhibitors are routinely added to aggressive environments to reduce metal dissolution and prolong service life [10]. Although many synthetic and inorganic inhibitors are effective, their toxicity, environmental persistence, and carcinogenic nature have raised serious health and ecological concerns. Consequently, there has been growing interest in developing environmentally benign alternatives [10-11].

Plant-based corrosion inhibitors have emerged as promising green substitutes due to their biodegradability, low toxicity, and rich phytochemical composition. Extracts derived from leaves, roots, seeds, and stems of various plants have demonstrated effective corrosion inhibition in acidic media. Several natural extracts—including tobacco, black pepper, *Nyctanthes arbor-tristis*, *Silybum marianum*, *Imperata cylindrica*, and *Newbouldia laevis*—have been successfully reported as corrosion inhibitors for steels and alloys [12-25].

The effectiveness of a corrosion inhibitor depends on factors such as availability, inhibition efficiency, solubility, cost, environmental compatibility and the employed extracting solvent. Since corrosion inhibitors are environment sensitive, it is essential to assess the aforementioned plant extract's inhibitory potential in a variety of pernicious settings. Thus, building on previous studies, the present work investigates the corrosion inhibition performance of mixed alcoholic extract of SG leaves as an environmentally compatible and sustainable green inhibitor for alloy 304L stainless steel in 1.0 M HCl solution. Gravimetric analysis, electrochemical measurements, and surface morphology characterization were employed to evaluate inhibitor performance and long-term stability.

2. MATERIALS AND METHODS

2.1. Alloy 304L Specimens and Materials Preparations

Rectangular specimens of alloy 304L stainless steel measuring 1 cm × 1 cm × 0.1 cm were prepared by mechanical cutting. Surface preparation was carried out by sequential grinding using silicon carbide abrasive papers ranging from 220 to 1200 grit in order to obtain a uniform and reproducible surface finish. The samples were subsequently degreased in ethanol, rinsed with acetone and bi-distilled water, and allowed to dry naturally at room temperature. To avoid atmospheric contamination prior to testing, all prepared specimens were stored in desiccators.

The corrosive medium consisted of 1.0 M hydrochloric acid prepared from analytical-grade HCl using double-distilled water. The nominal chemical composition of the alloy 304L stainless steel (wt.%) was 18.37 Cr, 8.01 Ni, 1.00 Mn, 0.39 Si, 0.03 C, 0.003 S, 0.04 P, with iron constituting the balance.

Fresh SG leaves were thoroughly washed and air-dried under shade for seventeen days. The dried leaves were pulverized and extracted in a mixture of Dichloromethane and Methanol (1:1) for 72 hours using a mass-to-solvent ratio of 4 g to 20 cm^3. After filtration, the solvent was removed by evaporation, yielding the crude extract, which was preserved at 273 K until use. Test solutions containing inhibitor concentrations between 0.2 and 1.4 g/L were prepared by dissolving appropriate quantities of the extract in the acidic medium. The phytochemical constituents of the extract were identified using GC–MS analysis. The outcome is shown in Table 1. Fig. 1 displays a few of the found phytochemical components in the SG extract

2.2. Measurement of Weight loss

Gravimetric measurements were performed by immersing pre-weighed alloy 304l specimens in 100 mL of the test solutions for a total duration of 60 days, with mass loss measurements recorded at ten-day intervals. After each exposure period, samples were retrieved, cleaned, dried, and reweighed. All tests were conducted in triplicate,

and the observed standard deviations remained below 5%, confirming acceptable reproducibility.

Eqs.(1) and (2) were used to compute the corrosion rate ($C.R_t$), and inhibition efficiency ($I.E_f$) [26].

$$C.R_t = \frac{87.6\, W^l}{D_s A\, T_i} \qquad (1)$$

Where W^l stands for the weight loss in mg, D_s stands for density of steel in g/cm^3, $A\ (cm^2)$ denotes the area, and, T_i (hr) is time of immersion.

$$I.E = \frac{(C.R_t)a-(C.R_t)p}{(C.R_t)a}\ x\ 100 \qquad (2)$$

Where (C.Rt)a and (C.R$_t$)p stand for the calculated corrosion rate (mm/y) in the absence and presence of the SG extract respectively

Correspondingly, the degree of surface coverage, Ɵ was appraised using (Eq. 3)in accordance with [27].

$$\theta = 1 - \frac{W_p^l}{W_a^l} \qquad (3)$$

Where W_p^l and W_a^l denote the respective weight loss (mg) in the presence and absence of the extract of SG.

It is of particular importance to note that the extended immersion duration of 60 days was intentionally selected to evaluate not only the short-term inhibition efficiency of the *Stylosanthes gracilis* (SG) extract but also its long-term stability and persistence under aggressive acidic conditions. While many corrosion studies involving green inhibitors are conducted over relatively short exposure periods ranging from a few hours to several days, industrial systems such as acid cleaning units, pickling baths, petrochemical process equipment, storage vessels, and heat exchangers may experience prolonged exposure to acidic environments. Consequently, long-duration gravimetric testing provides more realistic insight into the sustained protective capability of the inhibitor under service-like conditions.

2.2.1. Kinetic Evaluation

The mechanism and reaction pathways of the reaction are clarified by the kinetic assessment of corrosion inhibition. The corrosion process is primarily a heterogeneous reaction made up of anodic reactions that occur at the same or different rates. Using both first-order Eq. (4) and second-order kinetic models, the integral analysis method was used to analyze the inhibitor's kinetics [28].

$$-\frac{dC_{ss}}{dt} = K_1 C_{ss} \qquad (4)$$

The concentration of stainless steel is shown here by Css. By mathematically manipulating and integrating Eq. (4) at the borders of (Css)$_0$ and (Css)$_t$, where time t = 0 and t, Eq. (5) was obtained. Eq. (6) was then developed.

$$-Log\ [(Css)0 - (Css)t] = \frac{K_1\, t}{2.303} \qquad (5)$$

$$-Log\ (\Delta Wss) = \frac{K_1\, t}{2.303} \qquad (6)$$

The weight loss is represented by the parameter W$_{ss}$ in grammes (g), the immersion duration is represented by t in hours (h), and the constant for the first-order rate is denoted by k$_1$ in h^{-1}. The concentrations of stainless steel in the first and last stages using t = 0 and at a later time t are denoted by (C$_{ss}$)$_0$ and (C$_{ss}$)$_t$. Eq. (7) is used to ascertain, by way of calculation, the half-life alloy 304L for first-order kinetics.

Half − life expression,

$$t_{½} = \frac{0.693}{K_1} \qquad (7)$$

The following expression in Eq. (8) is the rate equation for the second-order kinetics.

$$-\frac{d[Css]t}{dt} = K_2\ (Css^2) \qquad (8)$$

The second-order rate constant, expressed in h^{-1}, is represented by the symbol k$_2$. The Eq. (8) becomes the following expression in Eq. (9) by way of transformation, when the integral version of Eq. (8) is used and boundary conditions are established from t = 0 to t = t and from (C$_{ss}$)t = 0 to (C$_{ss}$)t = (C$_{ss}$)t

$$\frac{1}{(Css)t} - \frac{1}{(Css)0} = K_2\, t \qquad (9)$$

The integral rate law of the second-order reaction is represented here, and its linear representation, displayed in Eq. (10), can be obtained by reformatting Eq. (9).

$$\frac{1}{\Delta Wss} = K_2\, t \qquad (10)$$

The formula to calculate the half-life of a reaction with second-order kinetics is given by Eq. (11).

$$t_{½} = \frac{1}{K_2 (Css)0} \qquad (11)$$

2.3. Electrochemical Measurements

Electrochemical measurements were carried out using a conventional three-electrode system connected to an Autolab VersaSTAT 4 potentiostat. Alloy 304L specimens embedded in epoxy resin with a 1 cm² exposed surface served as the working electrode, while platinum and Ag/AgCl electrodes were used as counter and reference electrodes, respectively. All experiments were conducted at 30 °C under aerated and unstirred conditions. Prior to polarization measurements, the working electrode was allowed to stabilize at open circuit potential for one hour. Potentiodynamic

polarization scans were recorded at a sweep rate of 1 mV/s within ±250 mV relative to the corrosion potential.

The corrosion potential (Ecorr) and corrosion current density (j_{corr}) were calculated using Tafel plots of potential vs log I. According to [29], the following formulas were used to calculate the corrosion rate ($C.R_t$), the degree of surface coverage (θ), and the percentage inhibition efficiency (percent IE):

$$C.R_t = \frac{0.00327\ x\ j_{corr\ x}\ eqv.wht}{D_s} \quad (12)$$

Where $C.R_t$ stands for the corrosion rate (mm/yr), j_{corr} (uA/cm^2) stands for corrosion current density, D_s (g/cm^3) denotes the density of steel, while, eqv.wht (g) represent specimen's equivalent weight.

From the values of the corrosion current density, the percentage inhibition efficiency (% IE) was evaluated in line with Eq. (13)

$$I.E = 1 - \left[\frac{j_{corr\ p}}{j_{corr\ a}}\right] 100 \quad (13)$$

Where $j_{corr\ p}$ and $j_{corr\ a}$ (mA/cm^2) are the corrosion current density in presence and absence of the SG extract.

Additionally, using the relationship in Eqs. (14 – 15) as suggested by [29], the Polarization Resistance (Rp) values were derived from the measured J_{corr} values.

$$B = \frac{bc\ ba}{2.303(bc+ba)} \quad (14)$$

Where bc (mV) denote Tafel cathodic slope, b_a (mV) signify Tafel anodic slope

$$R_p = \frac{B}{jcorr} \quad (15)$$

Where B is a constant.

2.4. Samples Characterization

Surface morphology before and after corrosion exposure was examined using a VEGA3 TESCAN scanning electron microscope to assess surface degradation and inhibitor film formation.

3. RESULTS AND DISCUSSION

3.1. GC–MS Analysis of Stylosanthes gracilis Extract

The corrosion inhibition performance of *Stylosanthes gracilis* (SG) extract can be directly related to the molecular structures and functional groups of the phytochemical constituents identified by GC–MS analysis. The effectiveness of plant-derived inhibitors is largely governed by the presence of heteroatoms (O, N, S, P), π-electron systems, aromatic or unsaturated bonds, hydrophobic hydrocarbon chains, and polar functional groups capable of adsorbing onto metallic surfaces and forming protective films.

The GC–MS results reveal that the SG extract contains several oxygen-, sulfur-, phosphorus-, and nitrogen-containing organic compounds with strong adsorption potential. These compounds collectively contribute to the high inhibition efficiency observed for Alloy 304L in 1.0 M HCl through synergistic adsorption and barrier film formation mechanisms.

The dominant constituent, 11-(2-Cyclopenten-1-yl) undecanoic acid (+)- (46.84%), appears to play a particularly important role in corrosion protection. This compound contains: a long hydrophobic hydrocarbon chain, a cyclopentene ring containing π-electrons, and a polar carboxylic acid (-COOH) functional group.

The carboxyl group can adsorb onto the alloy surface through donor–acceptor interactions involving oxygen lone-pair electrons and vacant d-orbitals of iron/chromium atoms, while the unsaturated cyclopentene ring enhances adsorption through π-electron interactions. Simultaneously, the long nonpolar hydrocarbon chain creates a hydrophobic barrier that restricts penetration of aggressive H^+ and Cl^- ions to the metal surface. Such amphiphilic behavior significantly improves surface coverage and inhibitor film compactness.

Similarly, Cyclopentaneundecanoic acid (16.32%) contributes to inhibition through its long-chain fatty acid structure. Fatty acid derivatives are well known for their ability to form densely packed adsorbed films on metallic surfaces due to strong van der Waals interactions between hydrocarbon tails. Although this compound lacks unsaturation compared with the cyclopentenyl derivative, its carboxyl functional group still provides strong adsorption capability through oxygen-containing active centers.

Sulfur-containing compounds identified in the extract, including Mercaptamine and Thiirane, are particularly significant because sulfur atoms possess high electron density and strong affinity for transition metals. Sulfur-containing organic molecules are recognized as highly effective corrosion inhibitors due to their ability to chemisorb strongly onto steel surfaces. In the acidic environment, sulfur atoms may coordinate directly with Fe atoms, forming stable metal–sulfur bonds that suppress anodic dissolution processes. Mercaptamine additionally contains an amino (-NH_2) group, introducing nitrogen lone-pair electrons that further enhance adsorption strength through synergistic N/S interactions.

The presence of oxygen-rich compounds such as: Oxirane-2,2'-(1,4-butanediyl)bis, 1,2:4,5:9,10-Triepoxydecane, and Methyl-4,6-ethylidene-α-D-galactopyranoside also contributes substantially to inhibition efficiency. Epoxide-containing compounds possess strained oxirane rings that exhibit high reactivity and strong adsorption

tendencies. Their oxygen atoms can donate lone-pair electrons to the vacant d-orbitals of surface metal atoms, promoting chemisorption and protective film formation. The galactopyranoside derivative contains multiple hydroxyl (-OH) groups that facilitate hydrogen bonding and electrostatic interactions at the metal/electrolyte interface, thereby improving adsorption stability.

Alcohol-containing compounds such as 3-Octen-1-ol (Z)- and 10-Undecyn-1-ol further enhance corrosion protection through hydroxyl functional groups capable of surface adsorption. Additionally, their unsaturated carbon bonds provide π-electron density that can interact with the metal surface. These compounds likely contribute to improved surface wettability and facilitate formation of a more coherent adsorbed inhibitor layer.

The identified Arachidonic acid, TMS derivative contains multiple unsaturated carbon bonds and oxygen-containing groups. Polyunsaturated compounds generally exhibit strong adsorption tendencies because π-electrons enhance donor–acceptor interactions with metallic surfaces. Moreover, the bulky hydrophobic structure may improve barrier properties by increasing film thickness and reducing diffusion of corrosive ions.

Compounds containing silicon functionalities, such as Trimethylsilyl-di(trimethylsiloxy)-silane, may additionally contribute to film stabilization. Organosilicon compounds are known to improve surface hydrophobicity and may enhance compactness of the adsorbed inhibitor layer through siloxane network interactions.

Nitrogen- and phosphorus-containing species, including 4-Nonene, 5-nitro- and Phosphonous dibromide, cyclohexyl-, also likely contribute to adsorption through lone-pair electron donation. Phosphorus-containing compounds are especially recognized for strong affinity toward metal surfaces and their ability to form protective phosphate-like interfacial complexes.

Overall, the corrosion inhibition performance of SG extract can therefore be attributed to the synergistic action of:

- oxygen-containing compounds enabling donor–acceptor adsorption,
- sulfur- and nitrogen-containing compounds promoting strong chemisorption,
- unsaturated π-electron systems enhancing surface interaction,
- hydrophobic long-chain fatty acids creating diffusion barriers, and
- multifunctional molecules improving film compactness and stability.

The coexistence of these phytochemical constituents explains the strong mixed-type inhibition behavior, high polarization resistance, and substantial reduction in corrosion current density observed experimentally. Rather than a single active molecule being responsible for inhibition, the protective performance of the SG extract arises from cooperative interactions among multiple phytochemical species adsorbing simultaneously on the Alloy 304L surface.

***T**able 1. Identified Phytochemical Ingredients in SG extract from GC/MS Characterization (Using a mixture of Dichloromethane and Methanol as Solvent)*

Name of Phytochemical Compound	Area (%)	Molecular Formula	Molecular Weight (g/mol)
Octanoic acid, silver(1+) salt	6.50	$C_8H_{16}AgO_2$	251.07
Mercaptamine	1.02	C_2H_7NS	77.15
Thiirane	0.56	C_2H_4S	60.12
11-(2-Cyclopenten-1-yl) undecanoic acid, (+)-	46.84	$C_{16}H_{28}O_2$	252.398
Oxirane-2,2'-(1,4-butanediyl)bis	3.33	$C_8H_{14}O_2$	142.195
Phosphonous dibromide, cyclohexyl-	0.72	$C_6H_{11}Br_2P$	273.93
1,6-Heptadiene, 3-methyl-	0.65	C_8H_{14}	110.2
Chloroacetic acid, 6-chlorohexyl ester	7.16	$C_8H_{14}Cl_2O_2$	213.10
1,2:4,5:9,10-Triepoxydecane	1.06	$C_{10}H_{16}O_3$	184.235
Cyclopentaneundecanoic acid	16.32	$C_{16}H_{30}O_2$	254.41
3-Octen-1-ol, (Z)-	1.12	$C_8H_{16}O$	128.2120
10-Undecyn-1-ol	2.59	$C_{11}H_{20}O$	168.28
Methyl-4,6-ethylidene-alpha.-d-galactopyranoside	4.23	$C_9H_{16}O_6$	220.221
Arachidonic acid, TMS derivative	1.93	$C_{23}H_{40}O_2Si$	376.6480
Trimethylsilyl-di(trimethylsiloxy)-silane	4.07	$C_9H_{27}O_2Si_4$	279.653
9-Decen-1-ol, pentafluoropropionat	0.49	$C_{13}H_{19}F_5O_2$	302.2808
Bicyclo[4.1.0]heptane,-3-cyclopropyl,-7-carbmethoxy, cis-	0.59	$C_{12}H_{18}O_2$	194.27
4-Nonene, 5-nitro-	0.80	$C_9H_{17}NO_2$	171.2368

The phytochemical compounds found in the SG extract is detailed in Table 1,

3.2. Gravimetric Investigation

3.2.1. Effect of SG leaves Extract on Corrosion Rate and Inhibition Efficiency

Table 2 lists the outcomes of exposing the alloy 304L to an aggressive 1.0 M HCl solution. Figs. (2 – 3) show, in relation to time, the corrosion propagation in alloy 304L and bahaviour of the extract of SG subjected to unfavourable 1.0 M HCl solutions with and without SG extract, while Figs. (3) and (4) show the behaviour of the extract concentration in relation to its protection efficiency and corrosion rate of the alloy 304L in the systems in which the extract was injected.

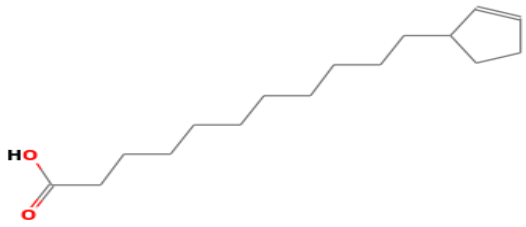

11-(2-Cyclopenten-1-yl) undecanoic acid, (+)- *($C_{16}H_{28}O_2$)*

Cyclopentaneundecanoic acid ($C_{16}H_{30}O_2$)

Figure 1. Chemical structure of a few chosen active ingredients in SG leaf extract

An in-depth analysis of the result reveal that exposure of alloy 304L steel to uninhibited 1.0 M HCl resulted in pronounced mass loss and rapid corrosion progression, confirming the aggressive nature of the chloride environment. However, the introduction of SG leaf extract led to a substantial reduction in corrosion severity across all exposure periods investigated.

The progressive reduction in corrosion rate with increasing SG extract concentration demonstrates the ability of the phytochemical constituents to suppress both metal dissolution and chloride-assisted passive film breakdown on Alloy 304L. The maximum inhibition efficiency of approximately 89.47% at 1.2 g/L compares favorably with several previously reported green inhibitors for stainless steels in acidic media.

For example, Soltani et al. reported inhibition efficiencies between 80–92% for *Salvia officinalis* extract on 304 stainless steel in 1 M HCl, attributing the protection to adsorption of oxygen-containing phytochemicals and aromatic compounds [4]. Similarly, Silybum marianum extract achieved inhibition efficiencies close to 90% for 304 stainless steel in HCl solution through mixed adsorption mechanisms involving flavonoids and phenolic compounds [15]. The inhibition performance obtained in the present work is therefore within the upper range of efficiencies commonly reported for plant-derived inhibitors acting on austenitic stainless steels.

Compared with other bio-based inhibitors previously investigated for 304L stainless steel, such as *Date Palm Waste* extract [44] and *Centrosema pubescens* extract [32], the SG extract exhibited superior long-term stability over the 60-day immersion period. This enhanced performance may be associated with the presence of long-chain fatty acid derivatives identified by GC–MS analysis, including cyclopentane undecanoic acid derivatives, which possess hydrophobic hydrocarbon tails capable of improving barrier film compactness and reducing electrolyte penetration.

The decline in inhibition efficiency beyond 1.2 g/L suggests that inhibitor performance is not solely concentration-dependent but also governed by adsorption equilibrium and intermolecular interactions at the metal surface. Similar deterioration at excessive inhibitor concentrations has been reported by Umoren et al. [46] and Loto et al. [41], where overcrowding of adsorbed species produced unstable multilayer adsorption and promoted partial desorption. This observation indicates that the adsorbed inhibitor layer likely transitioned from a compact monolayer arrangement to a less ordered structure at higher concentrations, thereby reducing film integrity.

Another important observation is the gradual decrease in inhibition efficiency with increasing immersion time. Although protection remained substantial throughout exposure, the reduction implies progressive weakening of the adsorbed film due to continuous chloride attack, desorption of weakly bound phytochemicals, and possible dissolution of corrosion products. This behavior is typical of predominantly physisorbed inhibitor systems and agrees with findings reported for other plant extracts in hydrochloric acid media [19,20]

Table 2. Outcomes of exposing the alloy 304L to an aggressive 1.0 M HCl solution

TIME	Conc (g/L)	C.R (mm/yr)	1.E (%)	Θ	- Log W.L	K_1	t ½ (h^{-1})	1/WL	K_2
10	Blank	1.77	0	0	-1.58	0.364	1.91	0.026	0.0026
10	0.2	0.93	47.37	0.4737	-1.30	0.300	2.31	0.05	0.005
10	0.4	0.70	60.53	0.6053	-1.18	0.271	2.56	0.067	0.0067
10	0.6	0.46	73.68	0.7368	-1	0.230	3.01	0.1	0.01
10	0.8	0.42	76.32	0.7632	-0.95	0.220	3.15	0.111	0.0111
10	1	0.33	81.58	0.8158	-0.85	0.195	3.56	0.143	0.0143
10	1.2	0.19	89.47	0.8947	-0.60	0.139	5.00	0.25	0.025
10	1.4	1.16	34.21	0.3421	-1.40	0.322	2.15	0.04	0.004
20	Blank	1.23	0	0	-1.72	0.199	3.49	0.019	0.0009
20	0.2	0.77	37.74	0.3774	-1.52	0.175	3.96	0.030	0.0015
20	0.4	0.56	54.72	0.5472	-1.38	0.159	4.36	0.042	0.0021
20	0.6	0.40	67.93	0.6793	-1.23	0.142	4.89	0.059	0.0029
20	0.8	0.37	69.81	0.6981	-1.20	0.139	5.00	0.063	0.0031
20	1	0.30	75.47	0.7547	-1.11	0.128	5.40	0.077	0.0039
20	1.2	0.19	84.91	0.8491	-0.90	0.104	6.66	0.125	0.0063
20	1.4	0.93	24.53	0.2453	-1.60	0.185	3.76	0.025	0.0013
30	Blank	1.10	0	0	-1.85	0.142	4.88	0.014	0.0005
30	0.2	0.77	29.58	0.2958	-1.70	0.130	5.31	0.02	0.0007
30	0.4	0.59	46.48	0.4648	-1.58	0.121	5.71	0.026	0.0009
30	0.6	0.45	59.16	0.5916	-1.46	0.112	6.17	0.035	0.0012
30	0.8	0.36	67.61	0.6761	-1.36	0.105	6.63	0.044	0.0015
30	1	0.30	73.24	0.7324	-1.28	0.098	7.06	0.053	0.0016
30	1.2	0.20	81.69	0.8169	-1.11	0.086	8.10	0.077	0.0026
30	1.4	0.87	21.13	0.2113	-1.75	0.134	5.16	0.018	0.0006
40	Blank	1.09	0	0	-1.97	0.114	6.10	0.011	0.0003
40	0.2	0.84	23.40	0.2340	-1.86	0.107	6.48	0.014	0.0005
40	0.4	0.64	41.49	0.4149	-1.74	0.100	6.92	0.018	0.0005
40	0.6	0.50	54.26	0.5426	-1.63	0.094	7.37	0.023	0.0006
40	0.8	0.38	64.89	0.6489	-1.52	0.087	7.93	0.030	0.0008
40	1	0.30	72.34	0.7234	-1.42	0.082	8.51	0.039	0.0010
40	1.2	0.21	80.85	0.8085	-1.26	0.072	9.59	0.056	0.0014
40	1.4	0.87	20.21	0.2021	-1.88	0.108	6.42	0.013	0.0003
50	Blank	0.99	0	0	-2.03	0.094	7.41	0.009	0.0002
50	0.2	0.79	20.56	0.2056	-1.93	0.089	7.80	0.012	0.0002
50	0.4	0.62	37.38	0.3738	-1.83	0.084	8.24	0.015	0.0003
50	0.6	0.48	51.40	0.5140	-1.72	0.079	8.77	0.019	0.0004
50	0.8	0.38	61.68	0.6168	-1.61	0.074	9.33	0.024	0.0005
50	1	0.30	70.09	0.7009	-1.51	0.069	10.00	0.031	0.0006
50	1.2	0.21	78.51	0.7851	-1.36	0.063	11.04	0.044	0.0009
50	1.4	0.82	17.76	0.1776	-1.95	0.090	7.74	0.011	0.0002
60	Blank	0.93	0	0	-2.08	0.080	8.68	0.008	0.0001
60	0.2	0.78	15.83	0.1583	-2.00	0.077	9.01	0.010	0.0002
60	0.4	0.61	34.17	0.3417	-1.90	0.073	9.51	0.013	0.0002
60	0.6	0.50	46.67	0.4667	-1.81	0.069	10.00	0.016	0.0003
60	0.8	0.38	59.17	0.5917	-1.69	0.065	10.68	0.020	0.0003
60	1	0.29	68.33	0.6833	-1.58	0.061	11.43	0.026	0.0004
60	1.2	0.21	77.5	0.775	-1.43	0.055	12.61	0.037	0.0006
60	1.4	0.80	14.17	0.1417	-2.01	0.077	8.97	0.010	0.0002

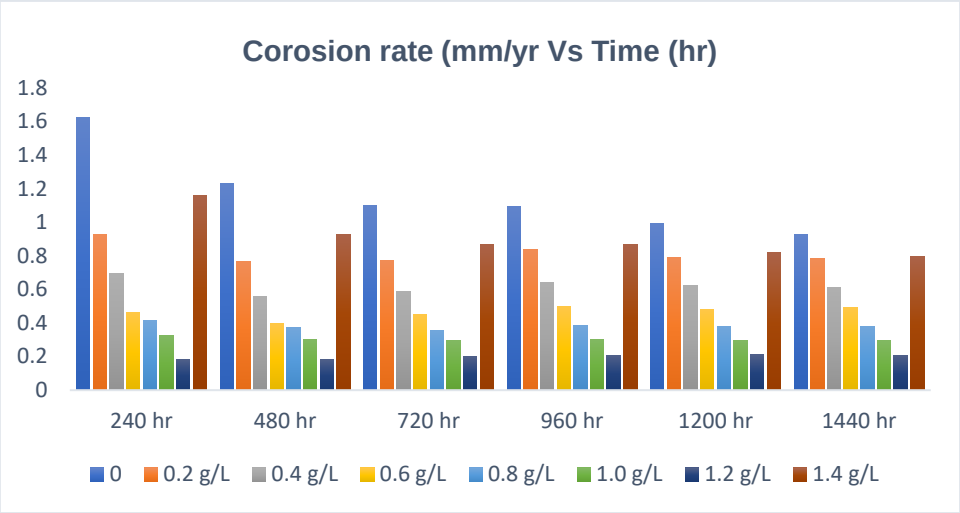

Figures 2. Shows corrosion propagation rate in alloy 304L, in relation to time, subjected to unfavourable 1.0 M HCl solutions without and with SG extract

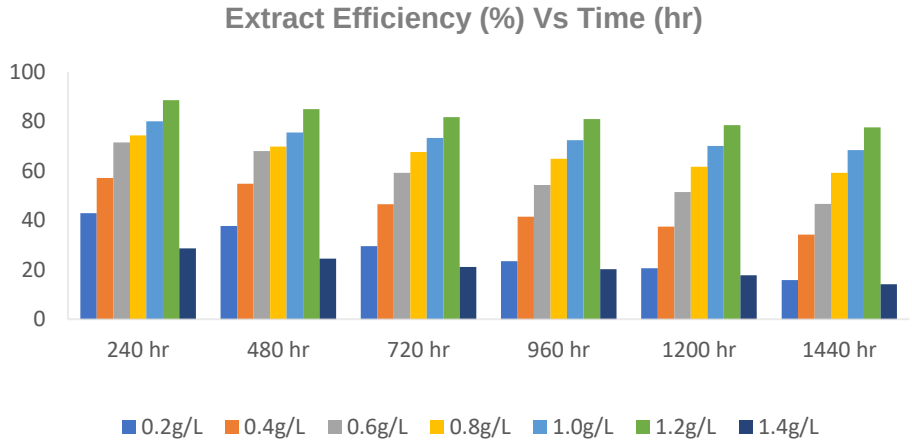

Figures 3. Shows inhibition efficiency of SG extract, in relation to time, during the corrosion of alloy 304L subjected to unfavourable 1.0 M HCl solutions without and with SG extract

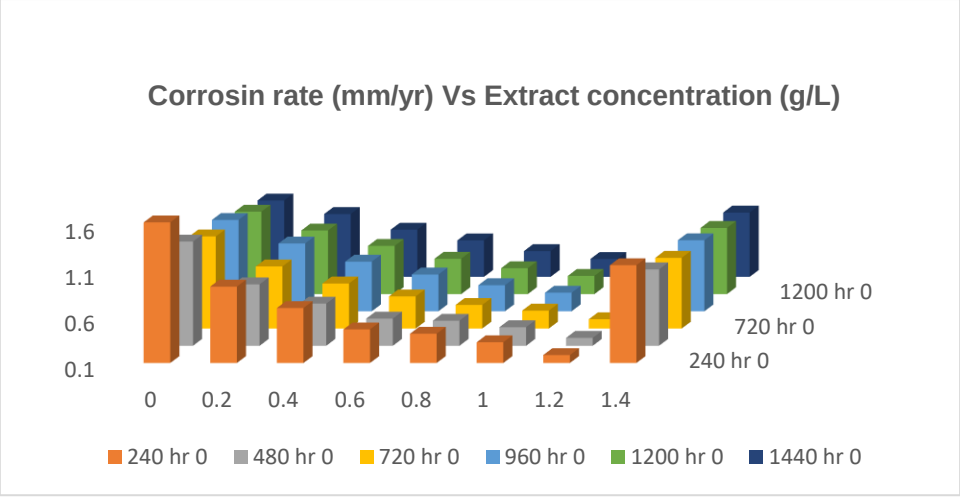

Figure 4. Show the relationship between corrosion rate and protection efficiency of SG Extract during the corrosion of alloy 30L in 1.0 M HCl solutions

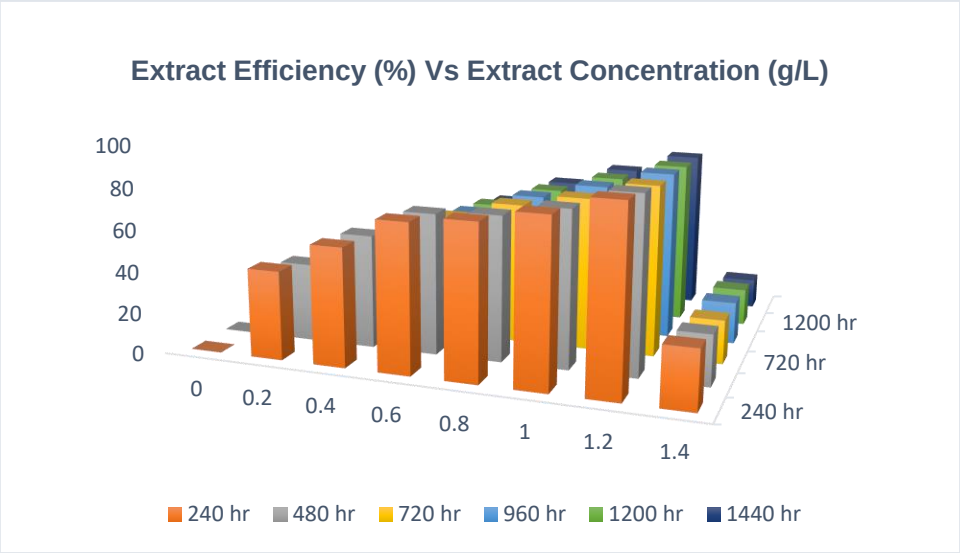

Figure 5. Show the dependency of inhibition efficiency on the concentration of the SG Extract during the corrosion of alloy 304L in 1.0 M HCl solutions

3.2.2. Kinetic evaluation of the Corrosion Process

To evaluate the experimental data, both first-order and second-order kinetic models were tested and applied. The resulting R2 values are summarized in Table 3, while the model fitting is illustrated in Figures 6a and 6b. For the corrosion of alloy 304L, tested both with and without varying concentrations of SG leaf extract, Fig. (6a) depicts the first-order plots of -Log (Δw) vs. time (hr), while Fig. (6b) represents the second-order plots of $\frac{1}{\Delta W}$ plotted against time (hr)

The kinetic results provide important mechanistic insight into the corrosion inhibition process. The higher correlation coefficients obtained for the first-order kinetic model indicate that corrosion propagation was governed in part by concentration-dependent surface reactions and not only diffusion-controlled mechanisms. Similar first-order corrosion kinetics have been reported for plant-derived inhibitors in acidic environments [28,30-34].

The reduction in rate constant and simultaneous increase in half-life with increasing SG concentration confirms that the extract substantially delayed electrochemical dissolution of Alloy 304L. Mechanistically, this implies that adsorption of SG constituents reduced the number of available active sites for charge transfer reactions. The inhibitor therefore altered the interfacial reaction pathway by increasing the activation barrier for metal dissolution.

Compared with uninhibited samples, the increase in half-life at optimum concentration indicates improved surface persistence of the passive/inhibitor hybrid film. This observation is particularly significant for stainless steels because corrosion in chloride media is often initiated through localized passive film rupture. The SG extract therefore appears not only to retard uniform corrosion but also to stabilize the chromium-rich passive layer against chloride-induced depassivation.

Table 3. R^2 values of the First and Second Order Kinetic Models During corrosion control of Alloy 304L in 1.0M HCl holding various amounts of the SG leaf Extract.

Kinetic order	BLANK	0.20 (g/L)	0.40 (g/L)	0.60 (g/L)	0.80 (g/L)	1.00 (g/L)	1.20 (g/L)	1.40 (g/L)
First Order	0.9488	0.9554	0.9603	0.956	0.9597	0.9462	0.938	0.9557
Second Order	0.8911	0.8386	0.8489	0.8258	0.8254	0.7999	0.772	0.8477

To further validate the kinetic interpretation of the corrosion inhibition process, the experimental gravimetric data were also fitted to second-order and El-Awady pseudo-first-order adsorption models. The goodness-of-fit of the various kinetic models was statistically evaluated using the Akaike Information Criterion (AIC) and Bayesian Information Criterion (BIC), Figure 7, which provide more rigorous model-selection criteria than correlation coefficients alone because they account for both fitting accuracy and model complexity.

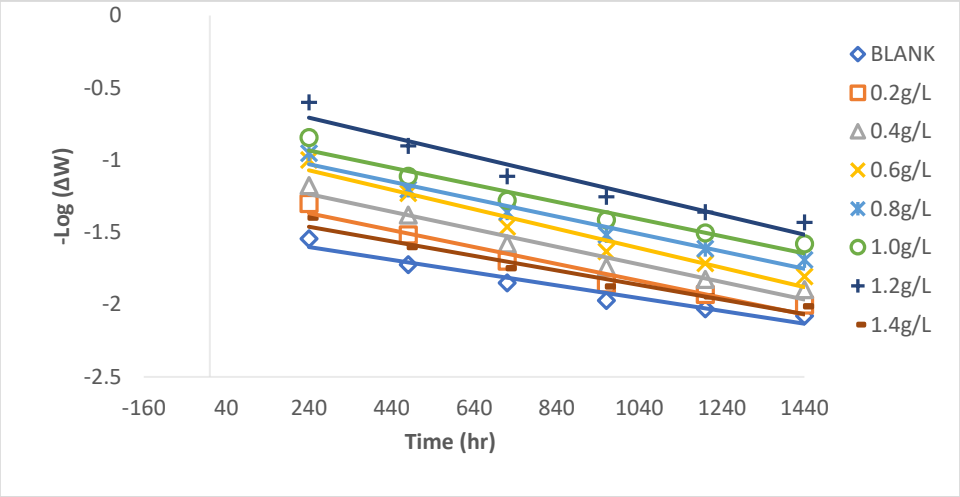

Figure 6a. First-order plot of -Log (Δw) Vs. Time (hr)

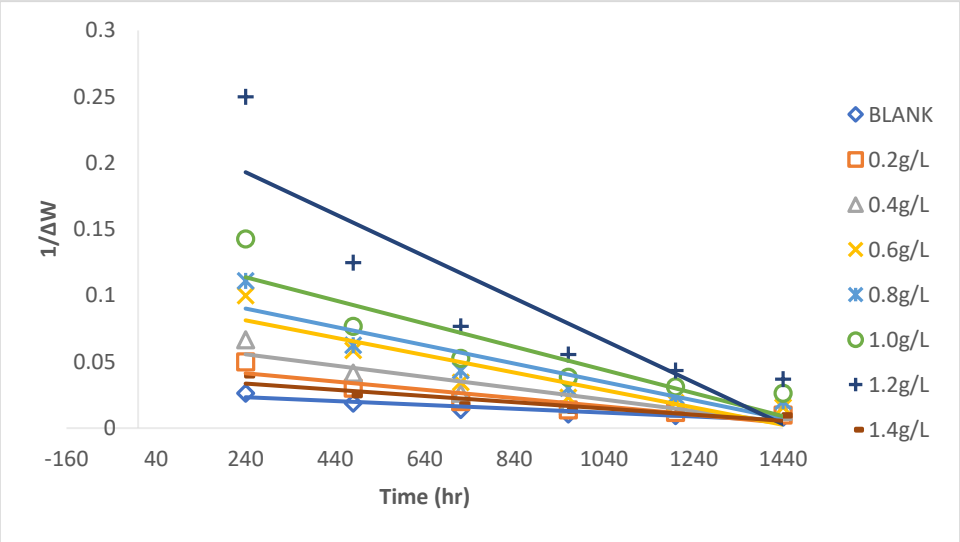

Figure 6b. Showing Second-order plot of $\frac{1}{\Delta W}$ Vs. Time (hr)

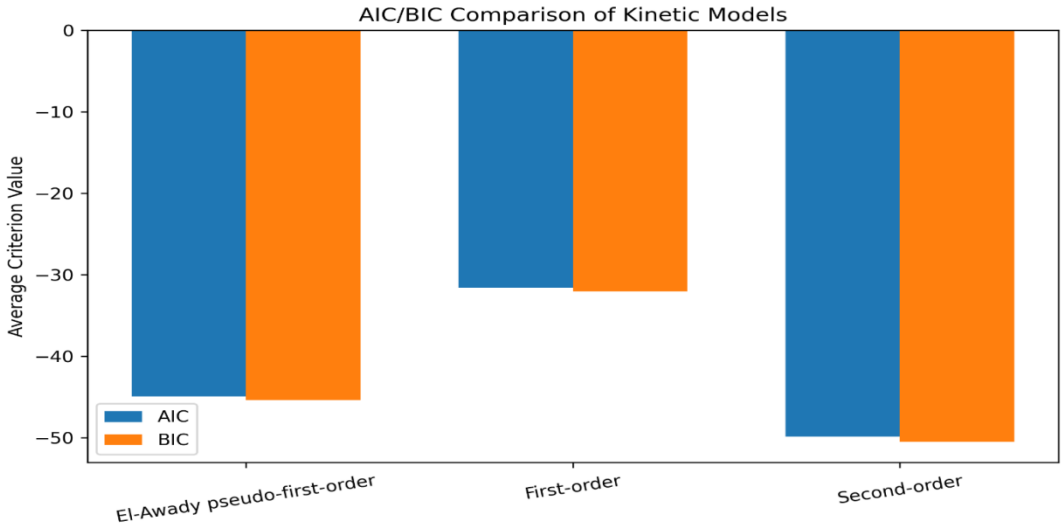

Figure 7. Showing AIC/BIC Comparison of Kinetic Models

The results showed that although the conventional first-order kinetic model produced relatively high correlation coefficients, the second-order model consistently yielded lower AIC and BIC values across most inhibitor concentrations. This indicates that the second-order model provided a statistically superior description of the corrosion process. The improved performance of the second-order model suggests that the corrosion inhibition mechanism may involve more complex surface interactions than simple concentration-dependent metal dissolution.

In corrosion systems involving plant-derived inhibitors, second-order behavior is often associated with adsorption-controlled processes involving interactions between multiple adsorbed species, surface rearrangement of inhibitor molecules, or cooperative adsorption phenomena. The phytochemical constituents present in the SG extract contain several oxygen-, sulphur-, and nitrogen-containing functional groups capable of forming intermolecular interactions on the Alloy 304L surface. Consequently, the adsorption process likely involved multilayer adsorption tendencies, lateral interactions among adsorbed species, and gradual restructuring of the protective film during prolonged immersion.

The El-Awady pseudo-first-order adsorption model also showed improved fitting performance compared with the conventional first-order model, indicating that adsorption equilibrium significantly influenced the corrosion kinetics.The suitability of this model therefore agrees with the slight deviations observed from ideal Langmuir adsorption behaviour and confirms that the inhibition process was strongly governed by adsorption–desorption dynamics at the alloy/electrolyte interface.

Despite the statistical superiority of the second-order model, the first-order kinetic approximation still retains mechanistic significance because the corrosion rate remained strongly dependent on the concentration of active metallic sites available for electrochemical attack. Therefore, the corrosion inhibition process may be interpreted as a predominantly adsorption-controlled electro-chemical process exhibiting mixed kinetic characteristics with contributions from both first-order surface-reaction behavior and second-order adsorption interactions.

The combined AIC/BIC analysis therefore provides deeper insight into the physicochemical complexity of the inhibition mechanism and demonstrates that corrosion protection by SG extract involves not only simple surface blocking but also cooperative adsorption and progressive stabilization of the inhibitor film over time.

3.2.2.1. Comparative Discussion of the Three Residual Plots

Residual analysis provides a more rigorous evaluation of kinetic model suitability because it reveals whether the fitted model adequately captures the underlying physicochemical behavior of the corrosion process. In the present study, residual plots were generated for the:

- conventional first-order kinetic model,
- second-order kinetic model, and
- El-Awady pseudo-first-order adsorption model.

A comparative assessment of the three residual distributions provides important mechanistic insight into the corrosion inhibition behaviour of Alloy 304L in 1.0 M HCl containing SG extract.

The residual plot for the conventional first-order model (Figure 8a) exhibited relatively larger residual magnitudes and mild systematic curvature, particularly at intermediate immersion periods (30–40 days). Although the residuals remained generally centered around zero, noticeable deviations from the baseline suggest that the first-order model could not fully account for all adsorption and interfacial processes occurring during corrosion inhibition. The presence of curved residual trends indicates that the corrosion process was more complex than a simple concentration-dependent surface dissolution mechanism. This observation implies that additional physicochemical interactions, such as adsorption heterogeneity and intermolecular effects among inhibitor species, contributed significantly to the inhibition process.

In contrast, the second-order residual plot (Figure 8b) displayed the smallest residual magnitudes and the most random distribution around the zero baseline. Most residual values remained within approximately ±0.02, substantially lower than those obtained from the first-order and El-Awady models. Furthermore, the residuals showed no pronounced systematic drift, clustering, or oscillatory behavior throughout the immersion period. Such random residual distribution strongly indicates that the second-order model successfully captured the dominant kinetics governing the corrosion inhibition process.

The superior performance of the second-order model suggests that corrosion inhibition by SG extract involved cooperative adsorption interactions among phytochemical molecules adsorbed on the Alloy 304L surface. The extract contains multiple active compounds possessing oxygen-, sulfur-, nitrogen-, and π-electron-containing functional groups capable of interacting simultaneously at the metal/electrolyte interface. Consequently, adsorption of one inhibitor molecule likely

influenced neighboring adsorption events, producing intermolecular interactions and non-ideal adsorption behavior consistent with second-order kinetics. The second-order model therefore appears to best describe the dynamic adsorption–desorption equilibrium and progressive stabilization of the protective inhibitor film.

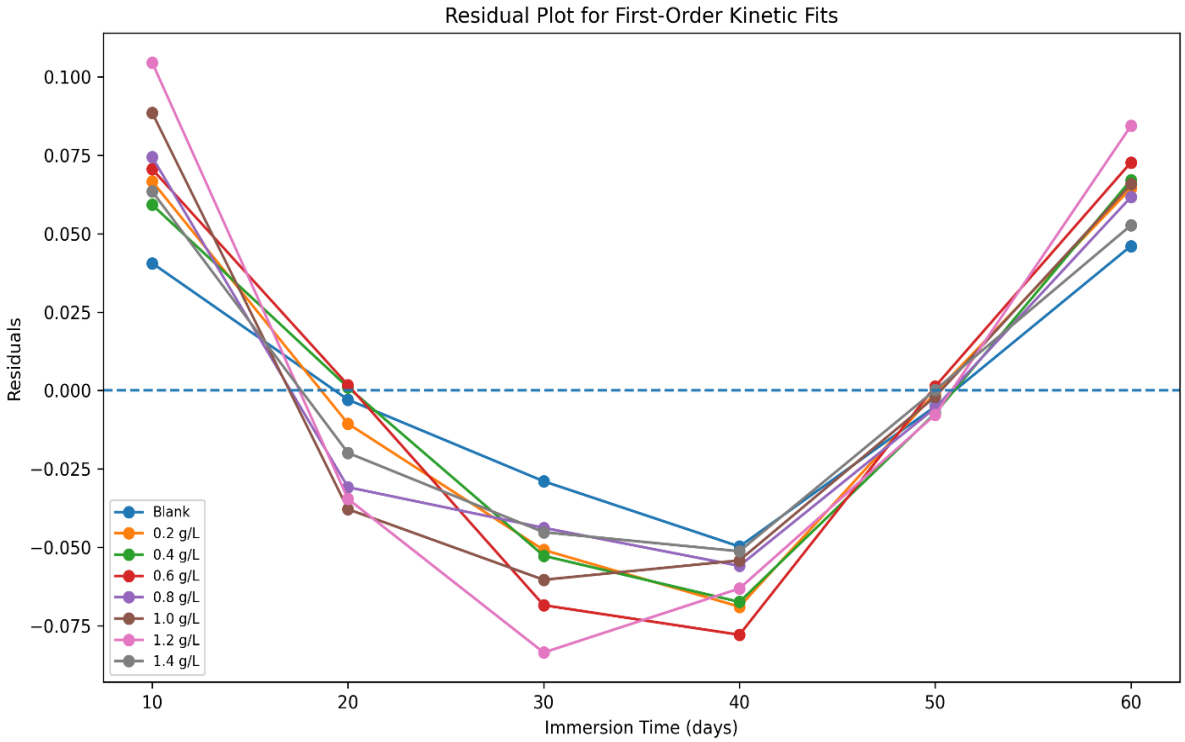

Figure 8a. Showing Residual Plots for First-order Kinetic Fits

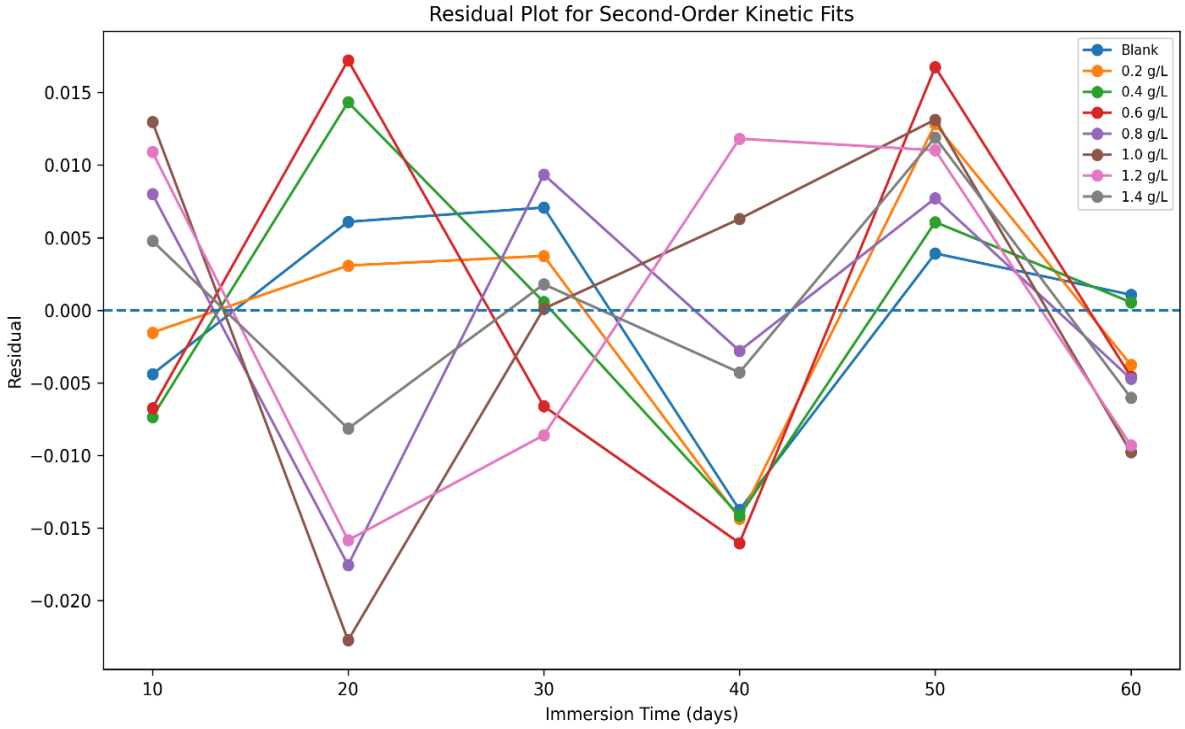

Figure 8b. Showing Residual Plots for Second - Order Kinetic Fits

The El-Awady pseudo-first-order adsorption model (Figure 8c) produced intermediate residual behavior between the first-order and second-order models. Although the residuals were generally moderate and remained close to the zero baseline, noticeable oscillatory patterns were observed at several immersion periods. Positive residual clustering at intermediate times followed by negative residuals at longer immersion durations suggests slight systematic deviation from ideal adsorption equilibrium. These deviations likely arose from gradual restructuring of the adsorbed inhibitor layer, heterogeneous occupation of active sites, and competitive adsorption among phytochemical constituents with different adsorption energies.

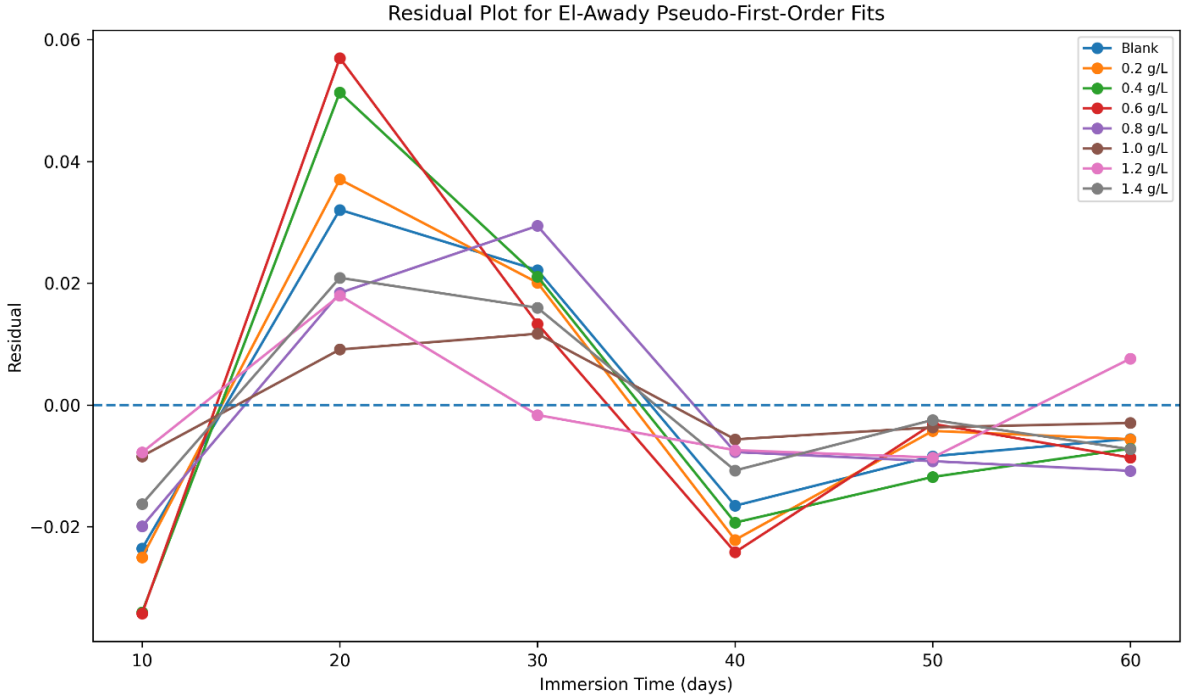

Figure 8c. Showing Residual Plots for El-Awady Pesudo-First Order Fits

Nevertheless, the relatively good performance of the El-Awady model confirms that adsorption equilibrium strongly influenced the corrosion inhibition process. The El-Awady model is particularly applicable to heterogeneous adsorption systems and multilayer adsorption behavior, both of which are expected in plant-derived inhibitor systems containing complex mixtures of phytochemicals. The residual trends therefore support the conclusion that the SG extract formed a heterogeneous protective adsorption layer rather than an ideal homogeneous monolayer.

When the three residual plots are considered collectively, a clear hierarchy in model suitability emerges:

Table 4. Comparative Discussion of the Three Residual Plots

Model	Residual Characteristics	Mechanistic Implication
First-order	Larger residual spread with mild curvature	Simplified surface-reaction approximation
El-Awady pseudo-first-order	Moderate oscillatory residuals	Adsorption-controlled heterogeneous surface behavior
Second-order	Smallest and most random residuals	Cooperative adsorption and strongest predictive capability

The combined residual analysis therefore demonstrates that the corrosion inhibition process cannot be fully explained by simple first-order metal dissolution kinetics alone. Instead, the inhibition mechanism involved:

- adsorption-controlled electrochemical reactions,

- cooperative interactions among adsorbed phytochemicals,
- heterogeneous surface occupation,
- dynamic adsorption–desorption equilibria, and
- progressive stabilization of the protective inhibitor film during prolonged immersion.

These findings are also fully consistent with:

- the Langmuir adsorption analysis,
- the high polarization resistance values,
- the mixed adsorption mechanism inferred from ΔG°ads,
- the SEM evidence of protective film formation, and
- the AIC/BIC statistical model comparison results.

Overall, the residual analyses provide strong statistical and mechanistic evidence that the second-order kinetic model offers the most realistic representation of the corrosion inhibition behavior of SG extract on Alloy 304L in hydrochloric acid medium.

3.3. Electrochemical Investigations

3.3.1. Open-circuit potential (OCP) Evaluation

To establish the open-circuit potential (OCP), a reference electrode was placed within the electrolyte in close proximity to the working metallic surface. The data confirmed that the experimental solutions achieved a steady state of equilibrium before any polarization measurement was conducted [58].

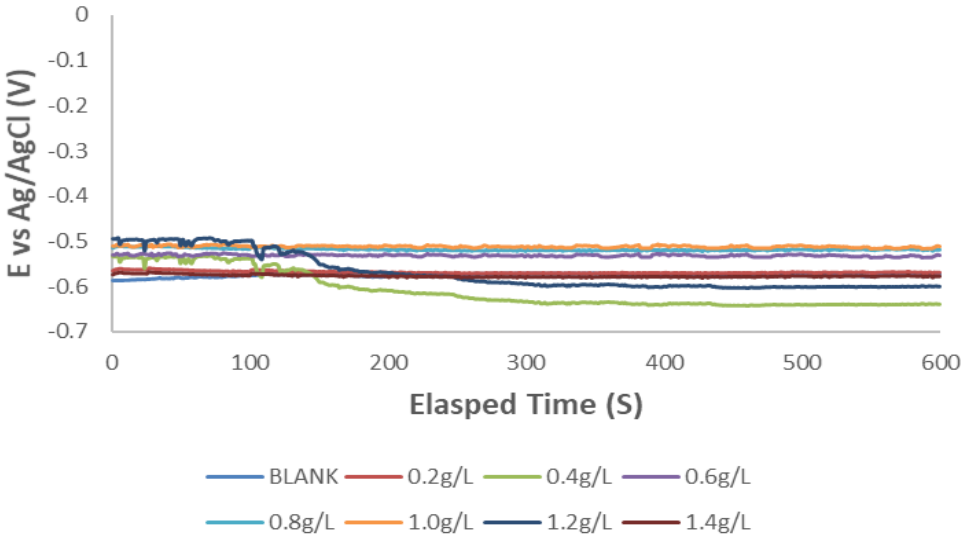

Figure 9. OCP Vs Time recorded for alloy 304L electrode in 1M HCl solutions containing varied concentration of SG extract at 30 ^{0}C.

As illustrated in Figure 9, the OCP readings exhibited initial fluctuations across all SG dosages but eventually reached a plateau. Notably, increasing the concentration of the extract caused the OCP to shift toward more noble (positive) potentials. This shift suggests that the SG extract acts as a mixed-type inhibitor, influencing both anodic and cathodic reactions [59,60]. This shift in electrochemical behaviour is likely attributed to the robust adsorption of the extract's bioactive molecules onto the metal surface.

The implication from the insightful survey of the results obtained show that the electrochemical investigations supported the gravimetric findings; showing that the conducted OCP measurements shifted toward more noble values upon SG extract addition, reflecting improved corrosion resistance.

3.3.2. Potentiodynamic polarization investigation

The potentiodynamic polarization curves for alloy 304L in 1.0 M HCl containing varying concentrations of SG leaf extract (Fig.10) reveal significant changes in both anodic and cathodic behaviour.The electrochemical parameters obtained from these measurements (Table 5) show a pronounced reduction in corrosion current density with increasing inhibitor concentration, indicating effective corrosion inhibition.

The polarization results strongly support the gravimetric observations and provide deeper insight into the electrochemical inhibition mechanism. The marked reduction in corrosion current density from 0.04048 to 0.00218 mA cm^{-2} demonstrates that the SG extract substantially suppressed the electrochemical kinetics of both

anodic metal dissolution and cathodic hydrogen evolution reactions [38 – 40].

The corrosion potential displacement of only 69 mV confirms that the extract behaved as a mixed-type inhibitor. According to electrochemical classification criteria, inhibitors producing Ecorr shifts below ±85 mV are generally categorized as mixed inhibitors because they influence both anodic and cathodic processes simultaneously rather than selectively blocking one half-reaction [29,41]. Similar mixed-mode behavior has been reported for *Silybum marianum* [15], *Date Palm Waste* extract [44], and *Gongronema latifollium* extract [58].

A particularly important finding is the dramatic increase in polarization resistance (Rp) from 296 to 6121 Ω·cm². Such a large increase indicates substantial obstruction of interfacial charge transfer processes and confirms formation of a compact adsorbed protective layer. Mechanistically, the increase in Rp suggests that the adsorbed phytochemical constituents created a barrier layer that:

- restricted electron transfer,
- reduced ionic mobility,
- displaced aggressive chloride ions from the alloy surface, and
- stabilized the passive chromium oxide film characteristic of Alloy 304L.

Table 5. Parameters of Potentiodynamic Polarization obtained during corrosion alloy 304L in 1.0M HCl with SG leaf extract in various concentrations

SG Concentration (g/L)	E_{corr} (mV)	bc (mV dec^{-1})	ba (mVdec^{-1})	j_{corr} (mA cm^{-2})	R_p (Ωcm^2)	C.R (mm/yr)	IE (%)	Θ
0	-588	49	63	0.0405	296	0.4699	0	0
0.2	-539	45	53	0.0106	997	0.1230	73.81	0.7381
0.4	-530	50	50	0.0084	1286	0.0980	79.15	0.7915
0.6	-524	45	48	0.0074	1370	0.0854	81.82	0.8182
0.8	-533	68	66	0.0058	2516	0.0671	85.72	0.8572
1	-526	98	87	0.0038	5211	0.0446	90.51	0.9051
1.2	-519	63	60	0.0023	6121	0.0253	94.62	0.9462
1.4	-529	115	87	0.0177	1212	0.2059	56.18	0.5618

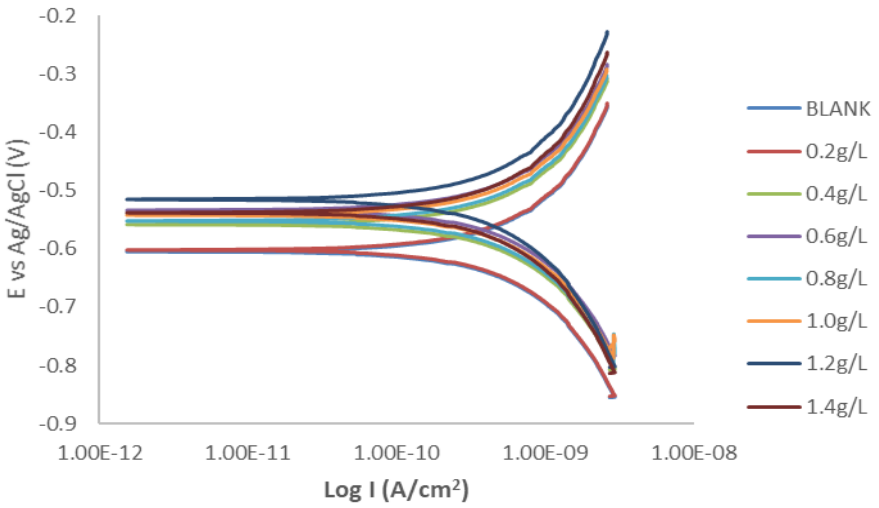

Figure 10. Polarization plot for alloy 304L corrosion in 1.0M HCl solution without and with SG leaf extract at 30°C

The decrease in both anodic and cathodic Tafel slopes also implies modification of the reaction pathways occurring at the alloy surface. This suggests that SG phytochemicals did not merely physically cover the surface but actively altered the activation energies associated with electrochemical reactions. Similar behavior has been linked to adsorption of heteroatom-containing organic compounds possessing π-electrons and lone-pair electrons capable of interacting with vacant d-orbitals of iron and chromium atoms [36,37].

The anodic Tafel slope (ba) and cathodic Tafel slope (bc) provide additional mechanistic insight into how the inhibitor modifies the electrochemical reactions occurring at the alloy surface. Variations in ba values suggest that adsorption of SG phytochemicals altered the anodic metal dissolution mechanism by blocking active anodic sites and increasing the activation energy required for oxidation reactions. Similarly, changes in bc indicate suppression of hydrogen evolution kinetics through adsorption of inhibitor molecules onto cathodic regions of the surface.

3.4. Investigation into Adsorption isotherm

By using certain adsorption isotherms, the corrosion inhibition mechanisms can be better understood. After fitting values into multiple isotherms in HCl solution, the Langmuir Isotherm best established the corrosion inhibition adsorption processes of the leaves extract SG on alloy 304L surface. A fit to the Langmuir isotherm was obtained by plotting a graph of C/Θ against C in accordance with Eq. (16).

$$\frac{C}{\theta} = \frac{1}{K_{ads}} + C \qquad (16)$$

Here K_{ads} (L/g) is known as equilibrium constant of adsorption, Θ is the extent of surface coverage, and C (g/L) denote the extracts concentration.

Table 6 shows the adsorption thermodynamic parameters, while Fig.(9)show the Langmuir plot.

Table 6. Langmuir adsorption and Thermodynamic parameters for the adsorption of the SG extracton the surface of alloy 304L in 1M HCl at 30 ^{0}C

Extract	Gradient	Intercept (gL^{-1})	K_{ads} (Lg^{-1})	R^2	ΔG^0_{ads} ($kJmol^{-1}$)
SG	0.9979	0.1042	9.60	0.99	-23.10

The following are the theories that underpin the Langmuir adsorption isotherm:

- The metal's surface has a consistent appearance.
- The adsorbate is adsorbed in a particular manner, with each adsorbed species occupying just one location on the surface.
- The adsorbed compounds do not disperse on the surface.
- The basic adsorption free energy is unaffected by the degree of coverage.

Straight line diagrams were collected as plots in all the cases with coefficient of determination, R^2 approximately unity. The strong conformity with the Langmuir adsorption isotherm suggests that adsorption occurred predominantly through formation of a relatively uniform adsorbed layer. However, the slight deviation of slope values from unity indicates that ideal monolayer assumptions were not fully satisfied. This discrepancy may be due to the inherent limitations of using the Langmuir adsorption isotherm to match data of traditional metal inhibition phenomena; for example, monolayer inhibitor adsorption is only possible on homogeneous metal surfaces with no adsorbed molecule diffusion at any temperature.That is, this deviation is common in corrosion systems involving complex plant extracts because multiple phytochemical species compete for adsorption sites while also interacting laterally with one another on the metal surface.

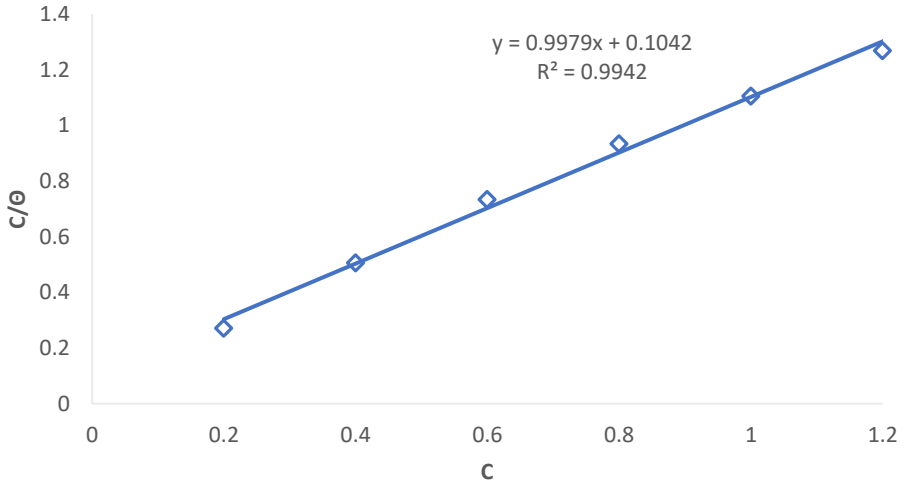

Figure 11. Langmuir adsorption isotherm for the extract of SG (0.2g/L – 1.2g/L) on alloy 304L surface in 1.0 M HCl solution

These assumptions, however, cannot be agreed for a conventional acid inhibition scheme, such as the one under consideration, since foreign ions and interactions may occur in the same solution; certain adsorption processes may also be potential dependent and selective in terms of the types of charges on the metal surface. In line with the assertion of [45-47], to understand these discrepancies in adsorption phenomena, another physical aspect of the adsorption isotherm must be considered. As a consequence, the Langmuir adsorption isotherm can be mathematically modified to account for the dimensionless separation constant, K_L, as defined in Eq. (17),

$$K_L = \frac{1}{1+K_{ads}\,C} \qquad (17)$$

where K_L denote the dimensionless extract adsorption separation factor, K_{ads} is the adsorptive/desorptive equilibrium constant and, C is SG extract's concentration. Table 6 show the measured K_L values for the extract of SG at 30 ^{0}C for alloy 304L in 1.0 M HCl. Values of K_L greater than 1 implies unfavourable conditions and are not compatible with the adsorption isotherm of Langmuir, while values of K_L less than 1, that is, $0 < K_L < 1$, indicate favourable conditions and are consistent with the adsorption isotherm of Langmuir, whereas, K_L values of 1 indicate an irreversible condition. Table 5 indicates that for all concentrations, all K_L values are less than one, meaning that the adsorption mechanism follows the adsorption isotherm of Langmuir.

The adsorption free energy, ΔG^0_{ads}, is proportional to the adsorptive/desorptive equilibrium constant (K_{ads}) [4] as follows:

$$K_{ads} = \left(\frac{1}{C_{solvent}}\right) exp\left(\frac{-\Delta G^0_{ads}}{RT}\right) \qquad (18)$$

Where R (Jmol^{-1}) = molar gas constant, T (K) = temperature, $C_{solvent}$ (gL^{-1}) = water concentration in solution, and K_{ads} (Lg^{-1}) = adsorptive/desorptive equilibrium constant found from the respective intercepts of Figure 9.

Table 7. Dimensionless separation constant, K_L, at the various concentrations of SG extract at 30 ^{0}C for alloy 304L in 1 M HCl

System (gL^{-1})	0.2	0.4	0.6	0.8	1.0	1.2	1.4	Mean
K_L	0.342	0.207	0.148	0.115	0.094	0.080	0.069	0.151

It's worth noting that $C_{solvent's}$ unit is determined by $K_{ads'}$. As shown in Tables 4, L g-1 is the unit of K_{ads}, implying that g/L is the unit of $C_{solvent}$, with an approximated value of 1.0×10^3 [48].

Tables 4 show that the calculated value of ΔG^0_{ads} is negative, connoting that the active molecules in the extract are adsorbing spontaneously.

Typically, ΔG^0_{ads} values in the range of -20 kJ mol^{-1} or lower are categorized as physisorption and those around -40 kJ mol^{-1} or higher are called chemisorption.

The calculated $\Delta G°_{ads}$ value of −23.10 kJ mol^{-1} provides important mechanistic information. This value lies within the transition region between physisorption and chemisorption, indicating that the adsorption process involved mixed adsorption behavior. Similar intermediate ΔG°ads values have been reported for many effective green inhibitors where electrostatic interactions coexist with donor–acceptor bonding [4,15,46].

The physisorption component likely arose from electrostatic attraction between protonated phytochemical species and the negatively charged metal surface, especially in the presence of adsorbed chloride ions. Simultaneously, chemisorption may have occurred through coordination between lone-pair electrons on oxygen-containing functional groups and vacant d-orbitals of surface iron/chromium atoms [29].

Thus, the presence of several active components in the extracts, some of which are adsorbed physically while others are adsorbed chemically, can further explain the complex mode of adsorption that combines both physisorption and chemisorption [49].

This dual adsorption mechanism is advantageous because physical adsorption facilitates rapid surface coverage while chemical adsorption enhances film stability and persistence. Such synergistic adsorption behavior may explain the relatively high inhibition efficiencies achieved by the SG extract.

3.5. Analysis of Surface Morphology and Elemental Composition

The Scanning Electron Microscopy (SEM) images in Fig. (12) illustrate the structural changes of the 304L alloy under different conditions: image (a) displays the metal after exposure to a 1 M HCl solution without protection, while image (b) shows the metal treated with 1.2 g/L of SG extract. Similarly, Figs. (13a and 13b) provide the Energy Dispersive X-ray (EDX) spectra for the untreated and treated samples, respectively.

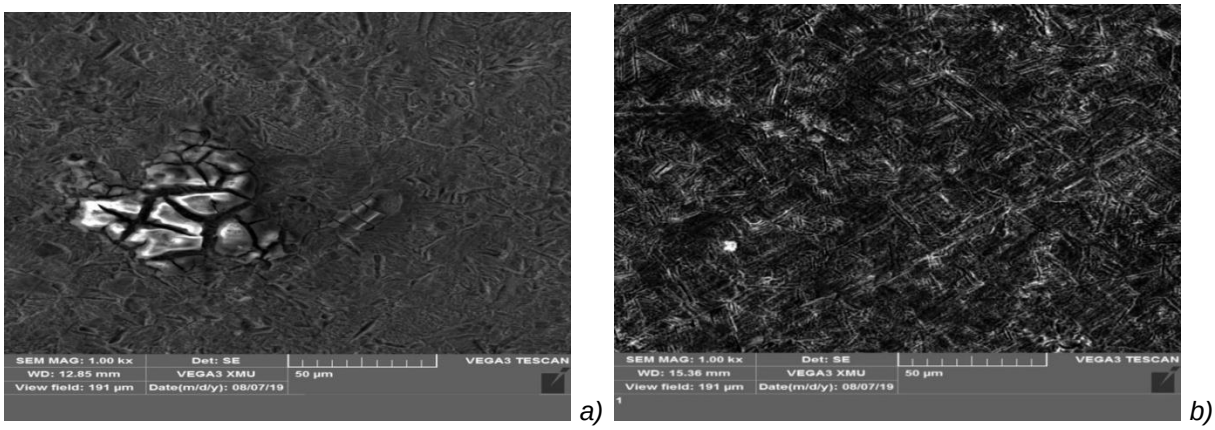

a) *b)*

Figure 12. SEM micrographs on the surface of alloy 304L: (a) Untreated alloy 304L in 1 M HCl, (b) Treated alloy 304L in the presence of 1.2 g/L of SG extract

3.5.1. Surface Morphology Observations

The SEM and EDX analyses provide direct physical evidence supporting the electrochemical and gravimetric findings. The severe pits and cracks observed on the uninhibited specimen are characteristic of chloride-induced localized corrosion resulting from passive film rupture and autocatalytic pit propagation.

In contrast, the inhibited specimen displayed a smoother and more homogeneous morphology, indicating that the SG extract effectively minimized surface degradation. Similar surface recovery effects have been reported for *Jasminum nudiflorum* extract [50], *Dendrocalamus brandisii* extract [51], and *Salvia officinalis* extract [4].

3.5.2. EDX and Elemental Analysis

The data in Table 8 and the spectra in Fig. 13 quantify the protective nature of the SG extract.

Table 8. Showing selected Elements of interest of EDS Analysis Result of alloy 304L in the absence and at optimum concentration of SG extract in 1 M HCl

Elements (wt. %)	C	O	Cl	Fe	Cr	Ni
Blank sample	11.99	46.80	1.35	7.34	1.93	1.98
Sample treated with SG	17.40	5.90	0.36	54.13	14.89	6.09

Since the extract is primarily composed of carbon (C) and oxygen (O), the shift in the weight percentages (wt. %) of C, O, and chlorine (Cl) serves as evidence for the inhibitor's adsorption onto the metal surface. Key findings include:

- Carbon and Chlorine Levels**:** Upon adding the extract, the carbon peak intensity increased while the chlorine peak diminished. This suggests that the inhibitor molecules are successfully displacing chloride ions [50].
- Oxygen Content**:** Oxygen levels were notably higher in the uninhibited acidic environment compared to the treated or polished samples, pointing to the formation of corrosion products in the absence of the extract [50].
- Iron, Chromium and Nickel Preservation: The EDX results show a dramatic difference in iron (Fe) content; the inhibited sample retained an Fe weight percentage of 54.13%, whereas the untreated sample plummeted to 7.34%[51]. In addition, the significantly higher retained Cr and Ni contents in the inhibited sample further demonstrate preservation of the alloy matrix and suppression of acid-induced dissolution.

These findings suggest that the SG extract formed a compact organic-inorganic hybrid film capable of reinforcing the native passive layer on Alloy 304L.

3.6.0. Mechanisms of Corrosion Inhibition

Organic inhibitors typically function by adsorbing onto a metal's surface, thereby modulating corrosion rates by suppressing anodic, cathodic, or mixed electrochemical reactions. The effectiveness and specific mechanism of this adsorption are influenced by several variables: the inhibitor's molecular architecture, the nature of the metal substrate, the specific interactions at the interface, and the composition of the corrosive medium [52].

The inhibition mechanism of SG extract can be explained through synergistic physicochemical interactions occurring at the alloy/electrolyte interface.

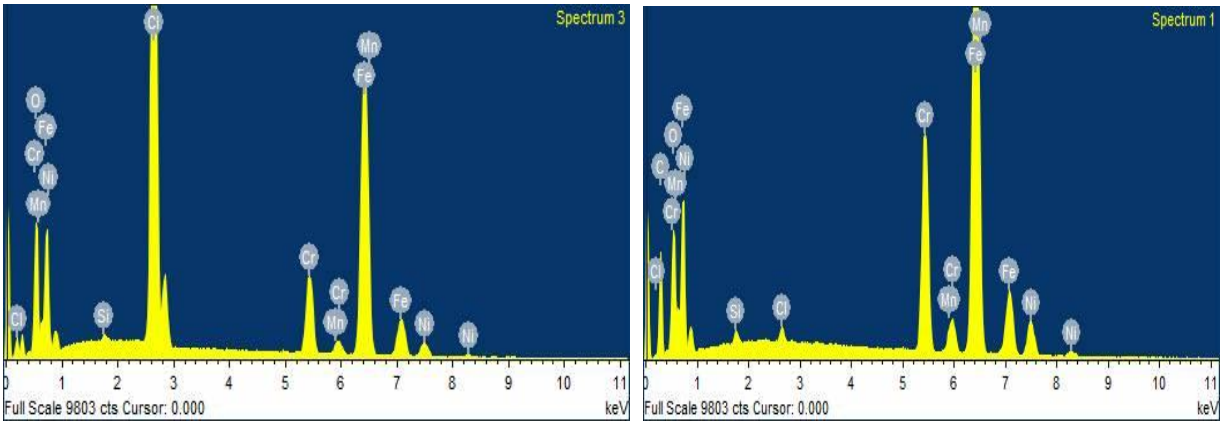

Figure 13. EDX Result on the surface of alloy 304L: (a) Untreated alloy 304L in 1 M HCl, (b) Treated alloy 304L in the presence of 1.2 g/L of SG extract

In acidic HCl solution, the phytochemical constituents become protonated and migrate toward the negatively charged metal surface already enriched with adsorbed chloride ions. Initial adsorption likely occurs through electrostatic attraction (physisorption). Subsequently, electron-rich functional groups such as hydroxyl, carbonyl, and carboxyl groups coordinate with vacant d-orbitals of Fe and Cr atoms, producing stronger chemisorptive interactions.

The identified fatty acid derivatives may additionally contribute hydrophobic hydrocarbon chains that orient outward from the surface, thereby creating a water-repellent barrier layer that restricts diffusion of H^+ and Cl^- ions toward the metal surface.

Beyond simple surface blocking, the inhibitor likely stabilizes the chromium oxide passive film characteristic of 304L stainless steel. Chloride ions typically penetrate defects in the passive film and initiate localized dissolution. Adsorption of SG molecules may reduce chloride adsorption, limit passive film rupture, and suppress pit nucleation.

Therefore, the corrosion inhibition process appears to involve multiple simultaneous mechanisms:

- electrostatic adsorption,
- donor–acceptor interactions,
- passive film stabilization,
- chloride displacement,
- hydrophobic barrier formation, and
- suppression of charge transfer kinetics.

This multi-mechanistic behavior explains the high inhibition efficiency and long-term protective performance observed for the SG extract system.

4. CONCLUSIONS

This study demonstrates that *Stylosanthes gracilis* (SG) leaf extract is an effective, environmentally friendly, and low-toxicity corrosion inhibitor for Alloy 304L stainless steel in 1.0 M HCl solution. The extract achieved a maximum inhibition efficiency of 94.6% at 1.2 g/L, forming a stable protective film that significantly reduced chloride-induced corrosion. Electrochemical, gravimetric, thermodynamic, kinetic, and surface analyses confirmed that SG acts as a mixed-type inhibitor, suppressing both anodic and cathodic reactions. Adsorption followed the Langmuir isotherm and proceeded through a combined physisorption–chemisorption mechanism.

A key novelty of this work is the demonstration of sustained corrosion protection over a prolonged 60-day exposure period under highly aggressive acidic conditions, highlighting the durability and practical potential of SG extract. The integration of kinetic modeling, adsorption studies, and statistical residual analyses provided deeper mechanistic insight into the inhibition process, revealing cooperative adsorption behavior and progressive stabilization of the protective film. GC–MS analysis further linked the inhibitor performance to the presence of heteroatom-containing and π-electron-rich phytochemical constituents responsible for enhanced surface protection.

The findings indicate strong potential for the application of SG extract in acid-handling industries, including pickling, descaling, petrochemical processing, and oil and gas operations, where it could serve as a sustainable alternative to conventional toxic inhibitors. Future studies should focus on identifying the most active phytochemical constituents, evaluating perfor-mance under industrial operating conditions, and

employing advanced surface characterization and computational techniques to further elucidate the inhibition mechanism. Overall, *Stylosanthes gracilis* extract shows considerable promise as a sustainable, high-performance corrosion inhibitor for stainless steel protection in acidic chloride environments.

5. REFERENCE

[1] B.O. Onyekpe (2002) Corrosion in oil and Gas Production. Ambik Press Benin City,

[2] M.N.C. Ljeoma (1991) Elements of Corrosion and Protection Theory. Auto Century Publication Co. Ltd, Enugu,

[3] M. Behpour, S.M. Ghoreishi, N. Khayat Kashani, N. Soltani (2009) Inhibition of 304 stainless steel corrosion in acidic solution by Ferula gumosa (galbanum) extract. Materials and Corrosion, 60(11), 895 – 898. http://dx.doi.org/10.1002/maco.200905182

[4] N. Soltani, N. Tavakkoli, M. Khayatkashani, M.R. Jalali, A. Mosavizade (2012) Green Approach to Corrosion inhibition of 304 stainless steel in hydrochloric acid solution by the extract of Salvia officinalis leaves. Corrosion Science, 62(1), 122-135.http://dx.doi.org/10.1016/j.corsci.2012.05.003

[5] R.V. Joseph Devaraj, V. Sivasangu, N. Sundharaj, D. A. Anbanantham, S.B. Moses, A. Aranganathan (2025) Adhutodavasica nees leaf extract as corrosion inhibitor for mild steel in acid medium. Zas. Materijala, 66 (2), 429 – 439. https://dx.doi.org/10.62638/ZasMat1219

[6] Z.A. Foroulis (1982) Corrosion and corrosion inhibition in the petroleum industry. Werkstoffe and Korrosion *33,* 121-131.

[7] J.I. Bregman, (1963) Corrosion Inhibitors, The MacMillan Company, New York

[8] T.A. Nguyen, X. Shi (2009) A mechanistic study of corrosion inhibiting admixtures.Anti-Corrosion Methods and Materials, 56(1), 3-12. http://doi.org/10.1108/00035590910923400

[9] F.M. Donahue, K. Nobe (1965) Theory of Organic Corrosion Inhibitors: Adsorption and Linear Free Energy Relationships. Journal of Electrochemical Society, 112, 886-891.http://doi.org/10.1149/1.2423723

[10] A.S. Fouda, A.S. Ellithy (2009) Inhibition effect of 4-phenylthiazole derivatives on corrosion of 304L stainless steel in HCl solution. Corrosion Science, 51, 868 – 875. http://doi.org/10.1016/j.corsci.2009.01.011

[11] B. A. Rani, B. B. J. Basu (2012) Green inhibitors for corrosion protection of metals and alloys: an overview. *International Journal of corrosion*, 1, 380217.http://doi.org/10.1155/2012/380217

[12] G.D. Davis, A.J. von Fraunhofer, L.A. Krebs, C.M. Dacres (2001) The use of Tobacco extracts as corrosion inhibitors. *CORROSION,* Paper 1558, http://doi.org/10.1016/j.porgcoat.2015.07.010

[13] R. Saratha, V.G. Vasudha (2009) Inhibition of Mild steel corrosion in 1N H_2SO_4 medium by acid extract of *Nyctanthesarbortristis* leaves. E-J.Chem.6 (4), 1003-1008.

[14] M.A. Quraishi, D.K. Yadav, I. Ahamad (2009) Green Approach to Corrosion Inhibition by Black Pepper Extract in Hydrochloric Acid Solution. The Open Corrosion Journal, 2, 56-60.

[15] N. Soltani, N. Tavakkoli, M. Khayat Kashani, A. Mosavizadeh, E.E Oguzie, M.R. Jalali (2014) *Silybummarianum* extract as a natural source inhibitor for 304 stainless steel corrosion in 1.0 M HCl. Journal of Industrial and Engineering Chemistry, 20 (5), 3217-3227. http://dx.doi.org/10.1016/j.jiec.2013.12.002

[16] O. E. Malomo, S. A. Yaro, D.S. Yawas, A.S. Akande, A. S. (2016) Inhibitive and Mechanical Properties of Cock's Comb and African Star Apple Leaves Extract on the Corrosion of Medium Carbon Low Alloy Steel In 1 M H_2SO_4 Solution. Annals of the Faculty of Engineering Hunedoara, 14(3), 39-48.

[17] O. Ofuyekpone, R.O Akaluzia, S. Edibo (2017) Investigating the influence Ofimmersion time and inhibitor concentration on the inhibiting potential of imperrata cylindrica as Corrosion Inhibitor of mild steel. International journal of research in engineering and innovation, 1(6), 147-152

[18] O.D. Ofuyekpone, E.S. Edibo, (2018) Investigating the Corrosion Resistance Behaviour of Zinc Metal–matrix Composite Reinforced with imperrata cylinderica.International Journal of Applied Research and Technology. *7(12*), 65 – 72.

[19] S.C. Udensi, E.O. Ekpe, L.A. Nnanna (2020) *Newbouldia laevis* Leaves Extract as Tenable Eco-Friendly Corrosion Inhibitor for Aluminium Alloy AA7075-T7351 in 1 M HCl Corrosive Environment: Gravimetric, Electrochemical and Thermodynamic Studies. Chemistry Africa,*3*(2), 303-316. https://doi.org/10.1007/s42250-020-00131-w

[20] P. S. Neriyana, V. D. Alva(2020) A Green Approach: Evaluation of Combretum indicum (CI) Leaf Extract as an Eco-friendly Corrosion Inhibitor for Mild Steel in 1M HCl. Chemistry Africa, 3(4), 1087-1098. https://doi.org/10.1007/s42250-020-00190-z

[21] K. Cissé, D. Gassama, A. Thiam, M. Bathily, M. Fall, (2021) Evaluationof the Inhibitory Effectiveness of Cyperus articulates Essential Oils on the Corrosion of Structural Steelwork in Hydrochloric Acid Solution. Chemistry Africa, 4(2), 379-390. https://dx.doi.org/10.1007/s42250-021-00229-9

[22] M. Benahmed, I. Selatnia, N. Djeddi, S. Akkal, H. Laouer (2019) Adsorption and Corrosion Inhibition Properties of Butanolic Extract of Elaeoselinum thapsioidesand Its Synergistic Effect with Reutera lutea (Desf.) Maires (Apiaceae) on A283 carbon Steel in Hydrochloric Acid Solution. Chemistry Africa, 3(3–4), 232-243, https://dx.doi.org/10.1007/s42250-019-00093-8

[23] R. Narasimha (2020) Green Compounds to Attenuate Aluminum Corrosion in HCl,Activation: A Necessity Review. Chemistry Africa 3,21–34. https://doi.org/10.1007/s42250-019-00114-6

[24] A. N. Pavel (2025) The inhibitory properties of the boiling extracts from Fagus sylvatica purpurea fallen leaves on the corrosion of mild steel in acidic environments. Zastita Materijala, 66(1), 206-214 https://dx.doi.org/10.62638/ZasMat999

[25] S.A. Abdlmanam, Elmaryami, A.A. Abdullah, A.M. Miftah, G. R. Rahel, O. S. AbdulHamid, M.S. Salah, A. Garret (2025) An evaluation of wood ashes as an eco-friendly environmentally corrosion inhibitor for low carbon steel in acidic solution at different temperatures. Zastita Materijala, 66 (2), 412 – 420. https://doi.org/10.62638/ZasMat1236

[26] R.T Loto, C.A. Loto, A.P.I. Popoola, T.I. Fedotova (2014) Inhibition Effect of 2-Amino, 5-Ethyl- 1, 3, 4 Thiadiazole onthe Corrosion of Austenitic Stainless Steel Type 304 in DiluteSulphuric Acid. Portugaliae Electrochimica Acta, 32(5), 337-354. https://doi.org/10.4152/pea.201405337

[27] P. Kumar, K.N. Mohana (2014) Phytochemical Screening and corrosion inhibitive behaviour of Pterolobium hexapetalum and Celosia argentea plant extracts on mild steel in industrial water medium. Egyptian Journal of Petroleum, 23, 201-211.http://doi.org/10.1016/j.ejpe.2014.05.007

[28] T.C. Egbosiuba, I.E. Chukwunyere, C.O. Awere, N.M Amadi, B.O. Okafor, J.O. Ezeugo, O.D. Onukwuli, N. Arrousse, E. Berdimurodov, V. C. Anadebe (2025), Psidium guajava L. extract as corrosion inhibitor for mild steel in an acidic environment: Experimental and computational insights. International Journal of Electrochem.Science, 20, 101031.https://doi.org/10.1016/j.ijoes.2025.101031

[29] M. Scendo, (2013) Adenine as an Effective Corrosion Inhibitor for Stainless Steel in Chloride Solution. International Journal of Electrochemical Science, 8, 9201-9221

[30] A.H. Al-Uqaily, R.A.H. Subhi Al-Bayaty, A.A. Khadom, M.K. Mustafa (2022) Inhibitive performance of 4-methoxyphenethylamine on low-carbon steel in 1 M hydrochloric acid: kinetics, theoretical, and mathematical views. J. Mol. Liq. 350, 118523.

[31] O. D.Ofuyekpone, A. A. Adediran, O. G. Utu, B. O. Onyekpe and U.G. Unueroh (2023) Non-toxic *leguminous* plant leaf extract as an effective corrosion inhibitor of UNS S30403 in 1M HCl. J. Electrochem. Sci. Eng. **13** (2), 231-250. http://dx.doi.org/10.5599/jese.1343.

[32] O.D. Ofuyekpone, O. G. Utu, B. O. Onyekpe, U. G. Unueroh, A. A. Adediran (2023) Corrosion Inhibition of Chloride-Induced Attack on AISI 304L Using Novel Corrosion Inhibitor: A Case Study of Extract of *Centrosema pubescens*. Chemistry Africa,**6,** 459-476.https://dx.doi.org/10.1007/s42250-022-00506-1

[33] O.D. Ofuyekpone, S.O. Okuma, S. Iweriolor, O.G. Utu (2025) Chemical Compounds from GC/MS Analysis, Functional Investigations, and Corrosion Inhibition Efficacy of a Bio-based and Sustainable Extract against HCl Solution-Activated Corrosion. *J Bio Tribo Corros,* 11, 37. https://doi.org/10.1007/s40735-025-00950-9

[34] O. D. Ofuyekpone, O. G. Utu, B.O. Onyekpe, A. A. Adediran, M. Oki (2020) Evaluation of protection performances of *Stylosanthes gracilis* extract against 304L corrosion in H_2SO_4 solution.Case Studies in Chemical and Environmental Engineering, 2,100058. https://doi.org/10.1016/j.cscee.2020.100058

[35] I.E. Uzoma, M.M. Solomon, R.T. Loto, S.A. Umoren (2022) Aspartame as a green and effective corrosion inhibitor for T95 carbon steel in 15 wt% HCl solution. Sustainability, 14 (11), 6500.

[36] M.M. Solomon, S.A. Umoren, M.A. Quraishi, M. Salman (2019) Myristic acid based imidazoline derivative as effective corrosion inhibitor for steel in 15% HCl medium. J. Colloid Interface Sci. 551, 47–60.

[37] M.M. Solomon, S.A. Umoren, M.A. Quraishi, D.B. Tripathy, E.J. Abai (2020) Effect of akyl chain length, flow, and temperature on the corrosion inhibition of carbonsteel in a simulated acidizing environment by an imidazoline-based inhibitor.J. Pet. Sci. Eng. 187, 106801

[38] M. Rajendran, T.S. Muthumegala, A. Krishnaven (2011) Green Corrosion Inhibitors- An Overview, Journal of Science and Industrial Research. Zaštita Materijala, 52(1), 1 -19

[39] V. Sribharathy, S. Rajendran, J. Sathyabama (2011) Inhibition of Mild Steel Corrosion in Seawater by Daucus carota. International Journal of Chemical Science and Technology, 1(3), 108 – 115.

[40] M. Shabani-Nooshabadi, M.S. Ghandchi (2015) Introducing the *Santolina chamaecyparissus* extract as a suitable green inhibitor for 304 stainless steel corrosion in strong acidic medium. Metallurgical and Materials Transactions A, 46(11), 5139-5148.

[41] R.T. Loto, C.A. Loto **(**2012)Effect of *P*-Phenylediamine on the Corrosion of Austenitic Stainless steel Type 304 in Hydrochloric Acid. International Journal of Electrochemical Science,7, 9423-9440.

[42] R.T. Loto, C.A. Loto, T. Fedotova (2012) Inhibition Effect of N, N'-Dimethylaminoethanol on the Corrosion of Austenitic Stainless Steel Type 304 in 3M H_2SO_4. International Journal of Electrochemical Science*,* 7, 10763-10778.

[43] R.T. Loto, C.A. Loto, A.P.I. Popoola(2012) Effect of Aminobenzene Concentrationson the Corrosion inhibition of Mild Steel in Sulphuric acid.International Journal of Electrochemical Science 7, 7016 – 7032.

[44] S. Sair, A. Oushabi, K. Nehhale, Y. Abboud, O. Tanane, A. El Bouari (2018) Date Palm Waste Extract as Corrosion Inhibitor for 304 Stainless Steel in 1 M HCl Solution.International Journal of Electrochemical Science*,* 13, 10642 – 10653. https://doi.org/10.20964/2018.11.38

[45] I. Dehri, M.O. ¨ zcan (2006) The effect of temperature on the corrosion of mild steel in acidic media in the presence of some sulphur-containing organic compounds. Materials Chemistry and Physics, 98 (2), 316–323, doi:10.1016/j.matchemphys.2005.09.020.

[46] S.A. Umoren, U.M. Eduok, A.U. Israel, I.B. Obot, and M.M. Solomon (2012) Coconut coir dust extract: a novel eco-friendly corrosion inhibitor for Al in HCl solutions. Green Chemistry Letters and Reviews, 5(3), 303-313. https://doi.org/10.1080/17518253.2011.625980

[49] S.A. Umoren, U.M. Eduok, A.P. Udoh (2012) Synergistic inhibition effects between leaves and stem extracts of Sida acuta and iodide ion for mild steel corrosion in1 M H_2SO_4 solutions. Arabian

Journal of Chemistry, 5, 325–337. https://doi.org/10.1016/j.arabjc.2010.09.006

[50] S. Deng, X. Li (2012)Inhibition by *Jasminum nudiflorum Lindl*.leaves extract of the corrosionof aluminium in HCl solution. *Corrosion Science*, 64, 253–262. https://doi.org/10.1016/j.corsci.2012.07.017

[51] X. Li, S. Deng (2012) Inhibition Effect of *Dendrocalamus brandisii* Leaves Extract on Aluminum in HCl, H_3PO_4 Solutions. Corrosion Science, 65, 299-308. https://doi.org/10.1016/j.corsci.2012.08.033

[52] N. I. Kairi, J. Kassim (2013) The Effect of Temperature on the Corrosion Inhibitionof Mild Steel in 1 M HCl Solution by Curcuma Longa Extract. Int. J. Electrochem. Sci., 8, 7138 – 7155

[53] K. Anbarasi (2018) Industrial application and inhibition properties of Cucurbita maxima on metal corrosion in aggressive medium. International Journal of Chemical Science, 2(1), 28-35

[54] O. Sanni, A.P.I. Popoola, O. S. I. Fayomi (2019) Temperature Effect, Activation Energies and Adsorption Studies of Waste Material as Stainless Steel Corrosion Inhibitor in Sulphuric Acid 0.5 M. Journal of Bio- and Tribo-Corrosion, 5,8-23. https://dx.doi.org/10.1007/s40735-019-0280-2.

[55] U.M. Eduok, M. Khaled (2015) Corrosion inhibition for low-carbon steel in 1 M H_2SO_4 solution by phenytoin: evaluation of the inhibition potency of another “anticorrosive drug”. Research in Chemical Intermediate **41**, 6309–6324. https://dx.doi.org/10.1007/s11164-014-1741-3

[56] R.T. Loto, C.A. Loto, A.P.I.Popoola, T. Fedotova (2015) Inhibition effect of butan-1-ol on the corrosion behaviour of austenitic stainless steel (type 304) in dilute sulphuric acid. Arabian Journal of Chemistry, http://dx.doi.org/10.1016/j.arabjc.2014.12.024.

[57] O.L. Riggs (Jr), R.M Hurd (1967) Temperature coefficient of corrosion inhibition, Corrosion, 23 (8), 252 -260.

[58] C.O. Akalezi, C.E. Ogukwe, E.A. Ejele, E.E. Oguzie (2016) Corrosion inhibition properties of *Gongronema latifollium* extract in acidic media. International Journal of Corrosion and Scale Inhibition, 5(3),232–247. https://dx.doi.org/10.17675/2305-6894-2016-5-3-4

IZVOD

UBLAŽAVANJE KOROZIJE LEGURE 304L U RASTVORU HCI KORIŠĆENJEM EKOLOŠKI KOMPATIBILNOG I ODRŽIVOG EKSTRAKTA

Ispitivanje performansi inhibicije korozije ekstrakta lista Stylosanthes gracilis (SG) na nerđajućem čeliku legure 304L u 1,0 M HCl je korišćenjem gravimetrijske, elektrohemijske, GC-MS, adsorpcije i SEM/EDX analize. Rezultati su pokazali da ekstrakt efikasno smanjuje koroziju formiranjem zaštitnog adsorbovanog filma na površini legure. Brzina korozije i gustina struje su se smanjivale sa povećanjem koncentracije ekstrakta, dok su se efikasnost inhibicije i otpornost na polarizaciju značajno povećavale, dostižući maksimalnu efikasnost od oko 94,6% pri 1,2 g/L. Pomeranje potencijala korozije od 0,069 V ukazuje na ponašanje inhibicije mešovitog tipa. Studije adsorpcije su otkrile spontanu adsorpciju prateći Langmirovu izotermu kroz kombinovane mehanizme fizisorpcije-hemisorpcije. Kinetičke i rezidualne analize su pokazale da model drugog reda najbolje opisuje proces inhibicije, što sugeriše kooperativne adsorpcione interakcije između fitohemijskih sastojaka. GC-MS analiza je identifikovala jedinjenja koja sadrže kiseonik, sumpor, azot i fosfor, odgovorna za adsorpciju i formiranje hidrofobne barijere.Rezultati SEM/EDX potvrdili su značajno smanjenje površinske degradacije izazvane hloridima. Studija pokazuje dugoročnu sposobnost zaštite od korozije i industrijski potencijal SG ekstrakta kao održivog zelenog inhibitora za nerđajući čelik u kiselim sredinama.

Ključne reči: *Inhibicija korozije, elektrohemijske tehnike, legura 304L, 1,0 M HCl, ekstrakt Stylosanthes gracilis*

Naučni rad
Rad primljen: 09.02.2026.
Rad korigovan: 20.05.2026.
Rad prihvaćen: 11.06.2026.

Okiemute Dickson Ofuyekpone https://orcid.org/0000-0002-0657-6372
Ngozi Grace Emordi https://orcid.org/0009-0005-7437-6232
Ochuko Goodluck Utu https://orcid.org/0000-0003-2656-3592
Adeolu Adesoji Adediran https://orcid.org/0000-0001-9457-1071

© 2026 Authors. Published by Engineering Society for Corrosion. This article is an open access article distributed under the terms and conditions of the Creative Commons Attribution 4.0 International license (https://creativecommons.org/licenses/by/4.0/)